Neutron deformation in ^{165}Ho

J. N. Knudson, J. D. Bowman, and S. I. Penttilä
Los Alamos National Laboratory, Los Alamos, New Mexico 87545

J. R. Comfort, J. Tinsley,* B. G. Ritchie, J. Görgen, and D. Mathis
Physics Department, Arizona State University, Tempe, Arizona 85287

S. S. Hanna, B. King,† and D. Počanić‡
Physics Department, Stanford University, Palo Alto, California 94305

R. A. Loveman§
Physics Department, University of Colorado, Boulder, Colorado 80309

L. S. Fritz and N. S. Dixon
Physics Department, Franklin and Marshall College, Lancaster, Pennsylvania 17604
(Received 21 March 1994)

We report asymmetries in the forward-angle differential cross sections for pion single-charge-exchange scattering from oriented and unoriented ^{165}Ho nuclei. These asymmetries are directly related to the neutron deformation of a nucleus that has a large charge quadrupole moment. The measured asymmetry extrapolated to 0° is -0.020 ± 0.024. In the model of Chiang and Johnson, this value implies a quadrupole deformation ratio $\beta_2^n/\beta_2^p = 0.84 \pm 0.08$, indicating that the excess neutrons are less deformed than the protons. This result conflicts with the predictions of the best available Hartree-Fock models based on Skyrme interactions. We also report on asymmetries of the nonresonant continuum and of the giant dipole resonances.

PACS number(s): 21.10.Gv, 21.60.Jz, 25.80.Gn, 27.70.+q

I. INTRODUCTION

The collective behavior of nucleons and the shapes of nuclei are some of the most basic and intensively studied issues in nuclear physics [1]. Charge distributions [2] have been determined and parameterized from extensive data obtained from electron scattering [3,4], Coulomb excitation [5–10], and muonic x-ray experiments [11,12]. Changes in mean-square nuclear charge radii are known from electronic K_α x-ray isotope shifts [13], optical isotope shifts [14,15], and Mössbauer isomer shifts [16]. Regions of spherical and permanently deformed nuclei are well delineated.

Charge-sensitive experiments, however, do not provide direct information on the shapes of neutron distributions. Although the nuclear symmetry potential acts to maintain similar proton and neutron distributions, differences may occur for at least two reasons. First, the neutrons are not influenced by the Coulomb potential which expands the proton distribution. Second, in heavy nuclei the excess neutrons populate orbitals that are largely empty of protons. The interplay between these competing factors is a subject of great importance for models of nuclear structure, both collective and microscopic. In the absence of clear information to the contrary, an equality between charge ($\simeq$ proton) and neutron distributions has commonly been assumed.

A. Proton and neutron deformations

Nuclear shapes are typically described by a multipole expansion of the radii in terms of spherical harmonics with coefficients β_L [1]:

$$R(\theta,\phi) = R_0[1 + \beta_2 Y_{20}(\theta) + \beta_4 Y_{40}(\theta) + \cdots]. \quad (1)$$

Elastic electron-scattering experiments provide the best systematic information on the nuclear shapes in that, to first order, the momentum-transfer dependence of the cross sections is the Fourier transform of the charge distribution. Auxiliary information and constraints are also obtained from inelastic-scattering experiments for which, within the framework of vibrational or rotational models, the cross sections are proportional to the squares of the β_L coefficients. The quadrupole deformation moment β_2

*Present address: EG&G/EM, 130 Robin Hill Road, Goleta, CA 93116.
†Present address: Institut de Physique Nucléaire et Centre de Recherches du Cyclotron, Université Catholique de Louvain, Louvain-La-Neuve, Belgium.
‡Present address: Department of Physics, University of Virginia, Charlottesville, VA 22901.
§Present address: Science Applications Corp., 2950 Patrick Henry Parkway, Santa Clara, CA 95054.

normally dominates for ground-state shapes and those of low-lying excitations.

Information on the shapes of the matter distribution may similarly be obtained from the scattering of hadrons. Most methods involve inelastic-scattering measurements and extraction of the β_L's by use of elaborate reaction calculations based on various models. The analysis is complicated by effects of the finite size of the probes which, when taken into account, tend to reduce discrepancies between the hadronic and electromagnetic results [17].

In view of the many difficulties, the results of the hadronic experiments are not always consistent. Thompson and Eck carefully examined data for a variety of probes from nucleons through ^{16}O on a series of targets between ^{12}C and ^{28}Si and concluded that hadronic and charge deformations were essentially equal [18]. In a similar analysis in the rare-earth region, Kuperin and Topil'skaya observed that there was equality between the charge and mass deformation parameters near the ends of the region, but that sizable differences in the middle of the region suggested a larger charge than matter quadrupole deformation [19]. However, Lee *et al.* argued in another study for nuclei in the same region that uncertainties in model assumptions precluded definite conclusions about relative shape differences [20]. In a recent study of low-energy neutron transmission on ^{165}Ho, Koster *et al.* concluded that the neutral and charged deformations are similar [21].

Data from inelastic polarized deuteron scattering produced agreement between electromagnetic and nuclear isoscalar transition rates for a variety of spherical nuclei, but showed differences of 10%–15% for several deformed nuclei [22]. Clement *et al.* suggested that nuclei in the latter case had smaller neutron than proton deformations. One of the nuclei was ^{152}Sm. However, Morris *et al.* found that pion scattering data from ^{152}Sm, for which the π^+ and π^- are predominantly sensitive to the neutron and proton deformations, respectively, appear to be consistent with equal deformations [23].

Theoretically, as shown by Brown, Madsen, and Anderson [24], deformations extracted from electromagnetic and hadronic inelastic-scattering vibrational transitions are expected to be different for nuclei with $N \neq Z$ due to the incomplete cancellation of the effects of a neutron excess by the symmetry potential. A mixing of isoscalar and isovector excitation modes is thus expected for different probes and should appear as small differences in β_L coefficients [24]. Such effects have been observed for (p,p') and (n,n') reactions on single-closed-shell nuclei by Bainum *et al.* [25,26] and by Finlay *et al.* [27].

B. A new approach

The interesting question of the present study is whether differences between neutron and proton deformations can be observed in the ground states of permanently deformed nuclei. Some Hartree-Fock calculations indicate that the ground-state charge and mass deformations should be nearly equal [28]. However, a recent study by Bartel, Johnson, and Singham suggests that observable differences may well exist, for example, in pion charge-exchange reactions to isobaric analog states (IAS) [29]. This suggestion was based on the earlier idea of Chiang and Johnson that the orientation asymmetry parameter

$$A_s = \frac{d\sigma^{\perp}/d\Omega - d\sigma^{\parallel}/d\Omega}{d\sigma^{\perp}/d\Omega + d\sigma^{\parallel}/d\Omega} \tag{2}$$

for the (π^+,π^0) charge-exchange reaction was very sensitive to the ratio of neutron and proton quadrupole deformations β_2^n/β_2^c [30]. In this equation, $d\sigma^{\parallel}/d\Omega$ and $d\sigma^{\perp}/d\Omega$ are the differential cross sections for the reaction with the symmetry axis of the deformed nucleus aligned parallel to or perpendicular to the beam direction, respectively.

Chiang and Johnson concluded in a subsequent study that the deformation ratio should also not be very sensitive to uncertainties in the reaction model [31]. Their argument is based on the fact that the transition density is determined by the spatial distribution of the excess neutrons, that resonance-energy pion reactions probe the nuclear surface, and that the distortions experienced by the pion are the same in both orientation states. This situation is different from that which usually pertains to reaction calculations with light or heavy ions. Specific application to the present experiment has been recently published [29].

C. Application

The nucleus chosen for the present study was ^{165}Ho. It has been frequently used to study "deformation effects" in nuclei with x-ray [12], neutron [32,33], electron [34–36], and pion [37] probes. At temperatures below 100 mK, the nuclear spin axes of the holmium nuclei are almost completely aligned in the basal planes of the crystal lattice [38], so that a single-crystalline sample can be aligned with the symmetry axis in a plane perpendicular to the beam direction without the use of an external magnetic field. Unfortunately, an alignment with the symmetry axis along the beam direction is prohibitively difficult to obtain. Thus a random orientation of nuclei was utilized instead and the measured asymmetry may be written as

$$A_r = \frac{d\sigma^{\perp}/d\Omega - d\sigma^{0}/d\Omega}{d\sigma^{\perp}/d\Omega + d\sigma^{0}/d\Omega}, \tag{3}$$

where $d\sigma^0/d\Omega$ is the cross section from the unoriented target. Although the sensitivity to the deformation is reduced by roughly a factor of three, this arrangement is feasible experimentally. Changes between the random and the aligned orientations could be obtained by changing the temperature from < 100 mK to > 3 K. Because there were no changes in the physical apparatus, and no changes in magnetic fields, this process minimized the systematic errors of the experiment.

A partial report of the data reported here has already been published [39]. The present paper provides full de-

tails of the experiment and the analysis of the data. New information is also presented with respect to the orientation asymmetry of the continuum and the giant dipole resonance.

II. EXPERIMENTAL PROCEDURES

The data were obtained with 165-MeV pions from in the Low Energy Pion channel at the Clinton P. Anderson Meson Physics Facility (LAMPF). The LAMPF π^0 spectrometer [40] was set in its one-post configuration and optimized for the detection of 155-MeV π^0's arising from the reaction ^{165}Ho$(\pi^+,\pi^0)^{165}$Er(IAS). The spectrometer was centered on a 0° scattering angle, with the distance between the target and the first photon conversion plane of each arm set to 110 cm. This configuration covered an angular range of 12° and was held fixed for the entire experiment. The energy resolution for monoenergetic π^0's was 2.6 MeV full width at half maximum. The momentum spread of the beam channel was set for $\Delta p/p = \pm 0.35\%$ (corresponding to an energy uncertainty $\Delta E = \pm 0.84$ MeV around the central beam momentum).

A. The target

The single-crystal metallic ^{165}Ho target was composed of two 1.2-mm-thick layers, with the first (second) layer consisting of a tightly packed mosaic of two (three) pieces of material [41]. All pieces were cut in a parallel fashion from a single ingot of high-purity single-crystal ^{165}Ho, and were oriented with the easy magnetization axes in the plane of the large face of the target. The ingot was not of a size sufficient to cover the entire area of the beam spot, which was approximately 2 cm vertical by 2.5 cm horizontal. The pieces were carefully cut and positioned for maximum coverage. There was very little if any spacing between adjacent pieces and, in any case, such spacings have no effect on the asymmetries. The two layers of target material were separated by 0.58 cm in order to compensate for the change in the opening angle of the π^0 decay with respect to finite target thickness against the average rate of energy loss in the target [40,42]. The target material was tightly clamped to a large copper frame.

The target assembly was mounted to the mixing chamber of a ^{3}He–^{4}He dilution refrigerator [43] which provided the required cooling. The temperature of the target frame was measured with a germanium diode resistance thermometer which was firmly attached to the copper frame, and whose resistance was determined by use of a sensitive bridge network. The target frame was maintained at a temperature of about 70–80 mK with the pion beam incident on the target. The beam of about 1.9×10^7 particles per second induced a temperature rise in the target assembly of about 20–30 mK, consistent with the expected energy loss.

In a test performed following the experiment, the temperature difference between the thermometer previously mentioned and a second germanium diode resistance thermometer mounted at the center of one layer of the target material was measured while the dilution refrigerator was cooled and operated. No temperature difference could be discerned at any time during the procedure, thus confirming that the target material was in good thermal contact with the mixing chamber of the refrigerator. The $d\sigma^{\perp}/d\Omega$ data were thus obtained by cooling the target to < 100 mK, while the $d\sigma^0/d\Omega$ data (i.e., unoriented) required warming the sample to > 3 K. All other experimental conditions remained the same, thus minimizing systematic errors.

The approximate alignment of the cryostat with respect to the beam was determined by survey methods. The actual position of the target was confirmed *in situ* by use of a "pi-ray" technique, in which a defocused beam made an image of the target, target frame, and cryostat components on photographic film. This image was compared with a similar image of the focused beam spot to determine that the focused beam hit the target during the experiment.

B. Shielding

Relatively large amounts of shielding were employed to reduce singles rates in the detector elements of the spectrometer arising from nontarget related beam interactions. A wall of lead bricks was situated upstream of the target area, and an additional massive wall of concrete and lead bricks was placed about two feet in front of the cryostat. A hut of lead bricks was also constructed around the end of the beam pipe to intercept beam halo and decay muons. These walls substantially reduced the background at the target due to decay muons and neutrons from the pion production target. Concrete blocks, with an opening to allow the beam to pass through, were placed downstream of the target and detectors. These blocks shielded the detector components from beam backscattered by the cave walls.

C. Data acquisition procedures

Data were acquired in multiple runs for each of the nuclear orientations (i.e., temperature settings). Because changes in the target temperature required several hours to complete, especially for lowering the temperature to less than 100 mK, each of these sets spanned approximately one week. Two separate "warm" and two separate "cold" sets of data were obtained. The individual runs were interspersed with periodic checks of the beam focus and position, as recorded on photographic film. The relative and absolute flux of the pion beam was monitored by using several techniques which are discussed in Sec. III C.

Backgrounds from the cryostat were determined from separate runs that employed a replica of the cryostat and target frame. Several runs with this dummy target were taken throughout the course of the experiment.

III. DATA ANALYSIS

A. Data reduction

The data were binned into four spectra by scattering angle for each target state. A Monte Carlo simulation [42] of the π^0 detection process was used to map the energy dependence of the detector solid angle at each scattering angle. The spectra of accumulated events were then converted into cross section spectra by a process that computed solid angles, efficiencies, attenuations, and target thickness on a channel-by-channel basis. Thus the counts in channel i, Y_i, are converted into a doubly differential cross section by using the following relation:

$$\frac{d^2\sigma}{d\Omega dE} = \frac{Y_i}{(\Phi \cdot \tau) \cdot \epsilon_{MW} \cdot \epsilon_c^{J\cdot K} \cdot \epsilon_F \cdot t \cdot a \cdot (\Delta\Omega)_i} \quad (4)$$

where Φ is the total π^+ flux incident on the target as determined by an ionization chamber (see Sec. III C), τ is the fraction of the integrated primary proton beam current incident on the target while the data acquisition system was live, ϵ_{MW} is the multiwire proportional chamber efficiency, $\epsilon_c^{J\cdot K}$ is the two-arm photon conversion efficiency [40], ϵ_F is the track reconstruction efficiency, t is the target areal density, a is the product of all photon attenuations, and $(\Delta\Omega)_i$ is the solid angle, which depends on the π^0 kinetic energy. The attenuation a takes into account the absorption of outgoing π^0 decay photons by the target, the aluminum walls of the cryostat (total thickness of 0.50 cm), and the 1.27-cm-thick polyethylene sheets placed in front of each arm of the spectrometer. The energy-dependent solid angle was determined numerically from the Monte Carlo results mentioned previously. The resulting spectra are shown in Fig. 1.

B. Fitting procedure

Following Erell *et al.* [44] the spectra were analyzed under the assumption that the cross sections may be decomposed into an isobaric analog state, a set of giant resonances, and a nonresonant component. The nonresonant part of the cross section varies linearly with the square of the momentum transfer, q^2, at fixed excitation energy, while the resonances have angular distributions that vary rapidly with q^2. A physical interpretation of this background behavior is given in Ref. [44].

We use the semiphenomenological function of Erell *et al.* [44], which was developed to treat the nonresonant part of the cross section of all of the spectra in a consistent manner. This function was designed to follow the energy and angle dependence of quasifree charge exchange scattering at large momentum transfer and includes a suppression factor for Pauli blocking. The function used is given by

$$\frac{d^2\sigma}{d\Omega dE} = N \frac{1 - e^{(E-E_o)/T}}{1 + [(E - E_{QF})/W_L]^2}. \quad (5)$$

The normalization N is a function only of q:

$$N = \frac{d\sigma}{d\Omega_o} A_0 \left[1 + A_1 \left(\frac{q}{k_F}\right)^2\right] \times \left\{\int \frac{1 - e^{(E-E_o)/T}}{1 + [(E - E_{QF})/W_L]^2} dE\right\}^{-1}, \quad (6)$$

where $d\sigma/d\Omega_o$ is the cross section for the elementary charge exchange process $\pi^- p \rightarrow \pi^0 n$, $E_{QF} = T_{\pi^0}(\pi^+ \mathrm{n} \rightarrow \pi^0 \mathrm{p}) - E_{CB}-$ proton binding energy, E_{CB} is the energy

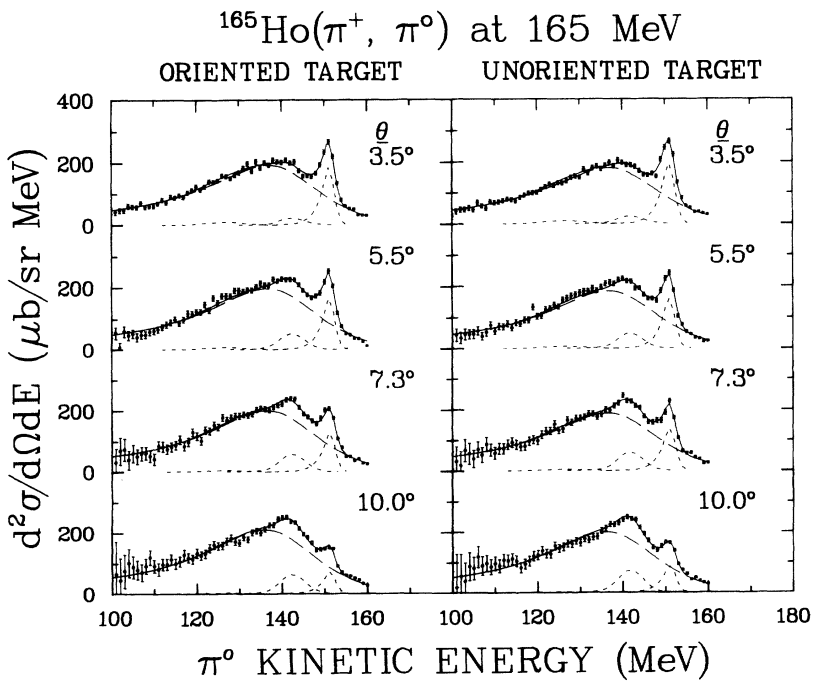

FIG. 1. Spectra for each alignment state. The dashed lines give the results of the fitting described in the text. The fits include contributions from a quasielastic background (long dashed line), an isovector monopole resonance (peaked at about 128 MeV in this figure), a giant dipole resonance (143 MeV), and an isobaric analog resonance (152 MeV).

associated with the Coulomb barrier of the struck proton $W_L = W_{L_0}[1 + \alpha(q/k_F)^2]$, E_0 is the Pauli-blocking cutoff energy parameter, and T is a cutoff energy scale parameter, with α and W_{L_0} taken as free parameters.

The line shape for the IAS and the resonances was taken to be that of a Gaussian central region with exponential tails, which closely reproduces both the line shape obtained from the Monte Carlo simulations and the observed line shape arising from monoenergetic peaks. The shape of the background is fully described in Ref. [44]. The location and width of the monopole resonance were fixed to values extrapolated from the systematics established in Ref. [44]. The location and width of the giant dipole resonance were allowed to vary, and did not deviate significantly from the systematics for these resonances. The location and width of the IAS were determined from the data.

The fitting procedure was done under two separate conditions: (a) with the angular distributions of the resonances allowed to vary freely, and (b) with the angular distributions constrained to follow $J_0^2(qR)$ and $J_1^2(qR)$ for the monopole and dipole, respectively. These methods gave no significant differences on the extraction of the IAS yields. The IAS area extractions also were not sensitive (to $< 1\%$) to details of the line shape used for the GDR, as we will discuss later. Typical fits are shown along with the data in Fig. 1. Figure 2 shows the IAS asymmetries A_r as a function of scattering angle.

We also investigated the consequences of the details of the shape of the GDR on the IAS area extraction. The GDR is known to be split [45] in the analog process ^{165}Ho(γ, n). We used a single peak for the GDR in the fits shown in Fig. 1; however, including provision for a split GDR in the fitting procedure, using parameters determined by Kelly *et al.*, makes a typically $< 1\%$ effect on the extracted IAS cross sections. As we will discuss in more detail later, the energy resolution of the π^0 spectrometer prevents us from determining whether double peaking in the isobaric analog of the ^{165}Ho dipole state is present in the charge-exchange case.

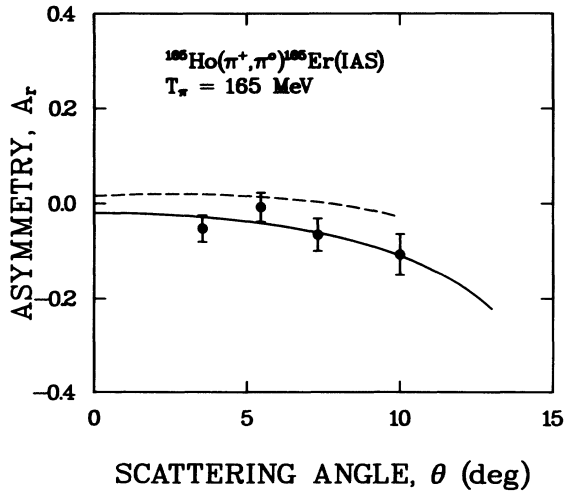

FIG. 2. Extracted asymmetries A_r as a function of angle θ. The smooth curve arises from fitting the aligned and unaligned cross sections with Eq. (8), then generating asymmetries with Eq. (3). The dashed curve is a coupled-channels prediction [29] of the asymmetry.

C. Yield normalizations

The extracted asymmetries do not depend on knowledge of the absolute beam intensity or the absolute solid angle of the detector. However, they do depend critically on the relative number of beam particles incident on the target between the "warm" and "cold" runs. This problem was addressed by placing an ionization chamber downstream of the cryostat in order to monitor fluctuations in the relative beam fluxes. The signals from the ionization chamber were digitized and scaled. Signals from two toroidal pickup coils around the primary proton beam from the accelerator were similarly scaled. Absolute flux normalizations were obtained from the activation of scintillator disks which provided cross-calibrations between the ionization chamber and the pickup coils [46].

To demonstrate the level of reliability of the beam normalization, Fig. 3 shows the distribution of the ratio

$$\frac{Y \cdot 10^8}{(\Phi \cdot \tau)\epsilon_{MW}} \tag{7}$$

for all of the "warm" and "cold" runs included in our data, where Y is the integrated yield in each run from 120 MeV to 160 MeV pion kinetic energy, and $\Phi \cdot \tau$ and ϵ_{MW} are defined in Sec. III A. This ratio includes all factors in Eq. (4) which can vary from run to run. The ratio is expected to remain constant, although the values for the "warm" data and "cold" data may differ. No significant time dependencies were observed. Variations in the ratio provide an empirical measure of the systematic errors in the experiment. Spurious runs, which could also be associated with poorly performing apparatus, were easily identified and excluded by use of this technique.

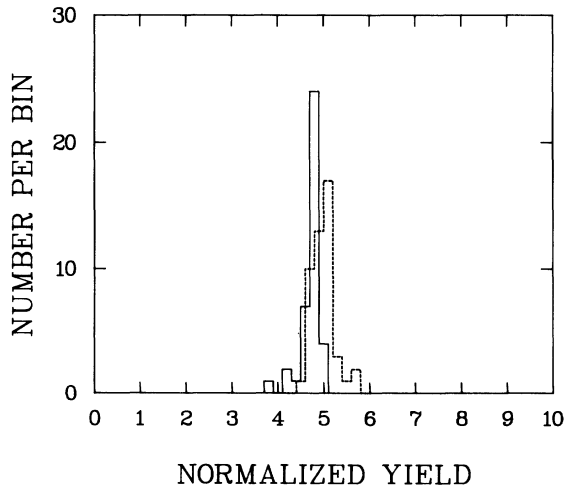

FIG. 3. Normalized yields $Y/(\Phi \cdot \tau)\epsilon_{MW}$. The solid line represents the unaligned ("warm") data runs; the dashed line represents the aligned ("cold") data runs.

Eliminating the five most extreme points from these distributions affects the basic result of this work, the ratio β_2^n/β_2^c, by about 13% of the quoted error bar.

The distribution for the set of 39 "warm" runs has a mean $\mu_{\rm warm} = 4.72$ and standard deviation $\sigma_{\rm warm} = 0.230$. The distribution for the set of 48 "cold" runs has a mean $\mu_{\rm cold} = 4.99$ and standard deviation $\sigma_{\rm cold} = 0.245$. The standard deviation of the relative pion flux between any two runs, i.e., σ/μ, is thus about 5%. However, the standard deviations of the means of the "warm" and "cold" runs, and hence the standard deviations of their respective sums, are about 0.04, or about 0.8%. The difference in the two means is thus significant.

IV. RESULTS

The main thrust of the experiment was to measure the orientation asymmetry for the isobaric analog transition; however, our spectra also contain information regarding the asymmetries of the nonresonant continuum and the resonances previously mentioned. Each of these topics will be discussed separately.

A. Isobaric analog state

The IAS cross sections for each target state, given in Table I, were fit to the function

$$\sigma(\theta) = a\left\{J_0^2(qR) + \frac{1}{2}(\Delta\theta)^2\,\frac{d^2}{d\theta^2}[J_0^2(qR)]\right\} \qquad (8)$$

as described in Ref. [44], where the overall amplitude a and the effective scattering radius R were fitting parameters. The second term accounts for the effects of the finite acceptance of the π^0 spectrometer. The parameters of a charged-matter Woods-Saxon distribution having an ellipsoidal surface are $R_0 = 6.15$ fm, skin thickness $a_s = 0.49$ fm, and $\beta_2^c = 0.32$ [12]. We obtain $a = 880 \pm 30$ μb/sr and 920 ± 40 μb/sr, with $R = 5.9 \pm 0.2$ fm and 5.4 ± 0.2 fm for the aligned and unaligned states, respectively. (These cross sections are about a factor of two smaller than those we reported earlier [44] due to an overall normalization problem with these data. We are confident that this problem does not affect the asymmetries we report here. We believe that the earlier cross sections remain correct.) The zero-degree asymmetry was determined from the values of $\sigma^{\perp}(0°)$ and $\sigma^0(0°)$. We obtain

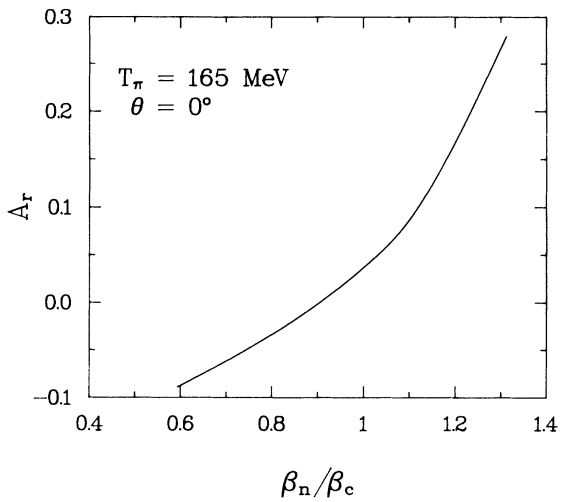

FIG. 4. The relationship between the ratio β_2^n/β_2^c and the asymmetry $A_r(0°)$ of Chiang and Johnson.

$$A_r(0°) = -0.022 \pm 0.024. \qquad (9)$$

Equation (3) was used with the values of a and R for the two target states to obtain the functional form of $A_r(\theta)$ shown in Fig. 2.

A value of the ratio β_2^n/β_2^c may be extracted from our value of $A_r(0°)$ by use of the model relationship obtained from the work of Chiang and Johnson [30], illustrated in Fig. 4. This Eikonal model is valid only at 0° and therefore does not predict an angular distribution for A_r. It is believed that the relationship is not very sensitive to parameter ambiguities [31]. We obtain

$$\beta_2^n/\beta_2^c = 0.84 \pm 0.08. \qquad (10)$$

Calculations have also been made with a model that employs deformed Hartree-Fock densities and a coupled-channels treatment of the reaction mechanism [29]. The dependence of $\sigma(0°)$ on β_2^n/β_2^c is believed to be qualitatively similar to that shown in Fig. 4, but differs in quantitative detail. However, these calculations have truncation uncertainties brought about by computational limitations and it is thought that the Eikonal results, which do not have such truncations, are perhaps a better representation of the 0° behavior [29].

On the other hand, the coupled-channels calculations predict an angular distribution that is shown as the

TABLE I. Cross sections for each orientation state for the isobaric analog state determined by fitting. The resulting asymmetry A_r is also shown.

Scattering angle, θ (deg)	Isobaric analog state cross section Oriented, $d\sigma^{\perp}/d\Omega$ (μb/sr)	Unoriented, $d\sigma^0/d\Omega$ (μb/sr)	Calculated asymmetry, A_r
3.5	744±30	826±32	-0.052±0.028
5.5	657±27	667±30	-0.0076±0.030
7.3	510±25	581±28	-0.065±0.034
10.0	294±19	364±21	-0.106±0.043

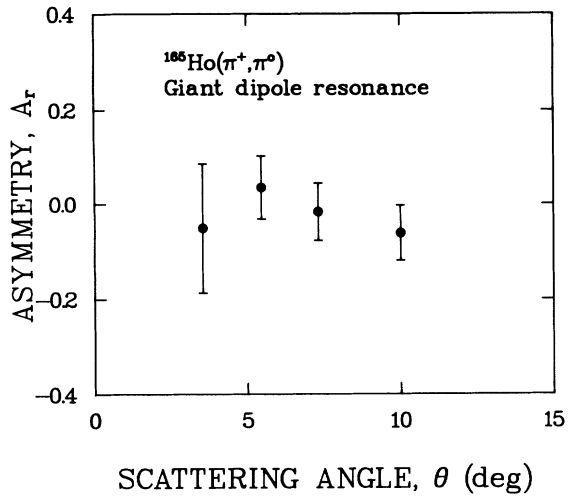

FIG. 5. Extracted asymmetries for the giant dipole resonance.

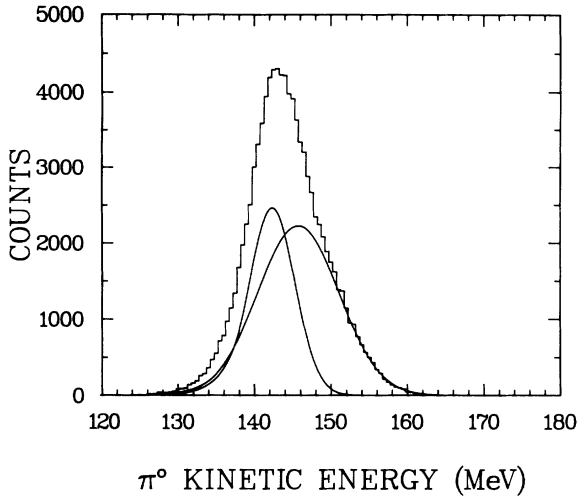

FIG. 6. Monte Carlo calculation of the expected lineshape (histogram) in the π^0 spectrometer arising from a two-component split of the giant dipole resonance (smooth curves).

dashed curve in Fig. 2 [29]. Again, the results are quite insensitive to parameter uncertainties [29]. The shape of the angular dependence of the asymmetry is similar to the data, although the magnitude of the calculation is systematically more positive than the data. The magnitude is a direct consequence of the fact that the calculation derives from a ratio $\beta_2^n/\beta_2^c \simeq 0.96$ [29]. The Hartree-Fock model calculations produced good agreement with observables such as charge radii and quadrupole moments, and two interactions gave approximately the same value of β_2^n/β_2^c [29]. In order to produce good agreement between the experimental and theoretical asymmetries, the relative normalization between the warm and cold data sets would have to be changed by 10%–20%, an amount well outside the known statistical and systematic uncertainties of our experiment.

Koster *et al.* [21] deduce a neutron deformation in ^{165}Ho from their measured matter deformation which does not agree with our result above. Their analysis utilized a neutron-nucleus optical potential with shape parameters substantially different from those deduced for the charge distribution from x-ray measurements [12]. The matter deformation was then combined with the charge deformation to infer a neutron deformation. Although deformation lengths $\beta_2 R_0$ were used instead of the deformation parameters β_2 themselves, it is possible that the effects of the different shape parameterizations have not been entirely compensated. No information about the sensitivity to the neutron optical potentials was given. The neutron deformation length of Koster *et al.* is larger than that of the protons which, if similar geometries apply, is opposite to the effects found by Kuperin and Topil'skaya [19], by Clement *et al.* [22], and in our work. The low-energy neutrons have a long wavelength and sample the nuclear volume, whereas the resonant energy pions are primarily sensitive to the nuclear surface and thus to small differences in shapes. We believe the analysis of the neutron experiment is subject to many of the same ambiguities and uncertainties as those of hadronic probes that were discussed in Sec. I A. In view of the rather low sensitivity of our result to the underlying reaction model, [31] we remain confident in the approach used in this paper.

B. Giant dipole resonance

We used the results of the fitting procedure described above to extract cross sections and to calculate asymme-

TABLE II. Cross sections for each orientation state for the giant dipole resonance determined by fitting. The resulting asymmetry A_r is also shown.

Scattering angle, θ (deg)	Giant dipole resonance cross section Oriented, $d\sigma^{\perp}/d\Omega$ (μb/sr)	Unoriented, $d\sigma^{0}/d\Omega$ (μb/sr)	Calculated asymmetry, A_r
3.5	167±44	185±47	-0.051±0.18
5.5	399±49	372±52	0.035±0.093
7.3	445±53	460±55	-0.017±0.084
10.0	488±55	552±50	-0.061±0.072

TABLE III. Cross sections for each orientation state for the nonresonant background determined by fitting. The resulting asymmetry A_r is also shown.

Scattering angle, θ (deg)	Cross section Oriented, $d\sigma^{\perp}/d\Omega$ (μb/sr)	Unoriented, $d\sigma^{0}/d\Omega$ (μb/sr)	Calculated asymmetry, A_r
3.5	4157±48	3898±52	0.032±0.0088
5.5	4228±49	3974±52	0.030±0.0088
7.3	4350±59	4101±52	0.029±0.010
10.0	4329±79	4379±83	-0.0056±0.013

tries of the giant dipole resonance. The cross sections and asymmetries are given in Table II, and the asymmetries are plotted in Fig. 5. The asymmetries are consistent with zero, although the statistical accuracy for the GDR is reduced by the relatively small peak and the large background. The 2.5-MeV resolution of the π^0 spectrometer prevents us from being able to see splitting of the GDR. Attempts at fitting the GDR with two peaks separated by 3.5 MeV, as seen by Kelly *et al.* [45] yielded ambiguous results. The Monte Carlo line shape code described above, when modified to simulate two peaks with parameters as noted by Kelly *et al.*, gave results consistent with the hypothesis that our spectrometer resolution was not adequate to resolve any such splitting of the GDR. These results are shown in Fig. 6, which depicts the individual input peaks (smooth curves) and how they would be perceived by our spectrometer (histogram).

C. Nonresonant background

The results of a similar analysis to that of the giant dipole resonance are given in Table III for the nonresonant background for π^0 kinetic energies between 110 MeV and 140 MeV. The asymmetries are shown in Fig. 7. The asymmetries in the background are nonzero, but the angular distribution is essentially flat. These nonzero asymmetries slightly exceed our stated uncertainty in the relative normalization between the aligned and the unaligned data. If these points were renormalized to be consistent with a zero asymmetry, then the IAS asymmetries would become more negative, with the resulting β_2^n/β_2^c being further from the Hartree-Fock prediction.

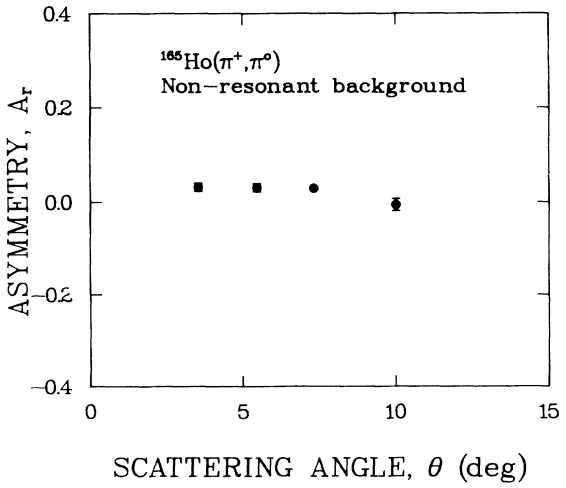

FIG. 7. Extracted asymmetries for the nonresonant background.

V. CONCLUSIONS

We have measured the asymmetries in forward-angle pion single-charge-exchange scattering from aligned and unaligned ^{165}Ho. On the basis of both intuitive arguments and detailed theoretical calculations, these asymmetries are found to be directly sensitive to the shape of the valence neutrons in a deformed nucleus such as ^{165}Ho. Although the ratio of deformation parameters depends on the application of a reaction model, our approach has been well examined and the sensitivity to model parameters is believed to be small [31].

We conclude that the neutron distribution in ^{165}Ho is considerably less deformed than the charge (proton) distribution, significantly less so than can be computed from the best available Hartree-Fock models. These data pose new challenges to models of nuclear structure and reaction mechanisms.

ACKNOWLEDGMENTS

We are indebted to Dr. Mikkel Johnson of LANL and Dr. Harvey Marshak, formerly with the National Bureau of Standards, for many helpful discussions. We also thank the staff at LAMPF for their assistance during the experiment. This work was supported by the DOE under Contract W-7405-ENG-36 and by the NSF under Grants DMR-8507915, PHY-8216201, and PHY-8520513.

[1] A. Bohr and B. Mottleson, *Nuclear Structure* (Benjamin, Reading, MA, 1975), Vol. II.
[2] J. L. Friar and J. W. Negele, in *Advances in Nuclear Physics*, edited by M. Baranger and E. Vogt (Plenum, New York, 1975), Vol. 8, p. 219.
[3] C. W. de Jager, H. de Vries, and C. de Vries, At. Data Nucl. Data Tables **14**, 479 (1974); **16**, 580(E) (1975).
[4] H. de Vries, C. W. de Jager, and C. de Vries, At. Data Nucl. Data Tables **36**, 495 (1987).
[5] K. E. G. Löbner, M. Vetter, and V. Hönig, Nucl. Data Tables **A7**, 495 (1970).
[6] D. L. Hendrie, N. K. Glendenning, B. G. Harvey, O. N. Jarvis, H. H. Duhm, J. Saudinos, and J. Mahoney, Phys. Lett. **26B**, 127 (1968).
[7] A. A. Aponick, C. M. Chesterfield, D. A. Bromley, and N. K. Glendenning, Nucl. Phys. **A159**, 367 (1970).
[8] F. S. Stephens, R. M. Diamond, and J. de Boer, Phys. Rev. Lett. **27**, 1151 (1971).
[9] T. K. Saylor, J. X. Saladin, I. Y. Lee, and K. A. Erb, Phys. Lett. **42B**, 51 (1972).
[10] C. E. Bemis, Jr., F. K. McGowan, J. L. C. Ford, Jr., W. T. Milner, P. H. Stelson, and R. L. Robinson, Phys. Rev. C **8**, 1466 (1973).
[11] R. Engfer, H. Schneuwly, J. L. Vuilleumier, H. K. Walter, and A. Zehnder, At. Data Nucl. Data Tables **14**, 509 (1974); **16**, 580(E) (1975).
[12] R. J. Powers, F. Boehm, P. Vogel, A. Zehnder, T. King, A. R. Kunselman, P. Roberson, P. Martin, G. H. Miller, R. E. Welsh, and D. A. Jenkins, Phys. Rev. Lett. **34**, 492 (1975).
[13] F. Boehm and P. L. Lee, At. Data Nucl. Data Tables **14**, 605 (1974); **16**, 580(E) (1975).
[14] K. Heilig and A. Steudel, At. Data Nucl. Data Tables **14**, 613 (1974).
[15] P. Aufmuth, K. Heilig, and A. Steudel, At. Data Nucl. Data Tables **37**, 455 (1987).
[16] G. M. Kalvius and G. K. Shenoy, At. Data Nucl. Data Tables **14**, 639 (1974).
[17] D. L. Hendrie, Phys. Rev. Lett. **31**, 478 (1973).
[18] W. J. Thompson and J. S. Eck, Phys. Lett. **67B**, 151 (1977).
[19] A. B. Kuperin and N. S. Topil'skaya, Sov. J. Nucl. Phys. **20**, 585 (1975).
[20] I. Y. Lee, J. X. Saladin, J. Holden, J. O'Brien, C. Baktash, C. Bemis, Jr., P. H. Stelson, F. K. McGowan, W. T. Milner, J. L. C. Ford, Jr., R. L. Robinson, and W. Tuttle, Phys. Rev. C **12**, 1483 (1975).
[21] J. E. Koster, C. R. Gould, D. G. Haase, and N. R. Roberson, Phys. Rev. C (to be published).
[22] H. Clement, R. Frick, G. Graw, F. Merz, H. J. Scheerer, P. Schiemenz, N. Seichert, and Sun Tsu Hsun, Phys. Rev. Lett. **48**, 1082 (1982).
[23] C. L. Morris, S. J. Seestrom-Morris, P. A. Seidl, R. R. Kiziah, and S. J. Greene, Phys. Rev. C **28**, 2165 (1983).
[24] V. R. Brown and V. A. Madsen, Phys. Rev. C **11**, 1298 (1975); V. A. Madsen, V. R. Brown, and J. D. Anderson, Phys. Rev. Lett. **34**, 1388 (1975); Phys. Rev. C **11**, 1298 (1975); **12**, 1205 (1975).
[25] D. E. Bainum, R. W. Finlay, J. Rapaport, J. D. Carlson, and J. R. Comfort, Phys. Rev. Lett. **39**, 443 (1977).
[26] D. E. Bainum, R. W. Finlay, J. Rapaport, M. N. Hadizadeh, J. D. Carlson, and J. R. Comfort, Nucl. Phys. **A311**, 492 (1978).
[27] R. W. Finlay, J. Rapaport, V. R. Brown, V. A. Madsen, and J. R. Comfort, Phys. Lett. **84B**, 169 (1979).
[28] H. Flocard, P. Quentin, and D. Vautherin, Phys. Lett. **B46**, 304 (1973).
[29] J. Bartel, Mikkel B. Johnson, and M. K. Singham, Ann. Phys. (N.Y.) **196**, 89 (1989).
[30] H.-C. Chiang and Mikkel B. Johnson, Phys. Rev. Lett. **53**, 1996 (1984).
[31] H.-C. Chiang and Mikkel B. Johnson, Phys. Rev. C **31**, 2140 (1985).
[32] R. Wagner, P. D. Miller, T. Tamura, and H. Marshak, Phys. Rev. **139**, B29 (1965).
[33] T. R. Fisher, R. S. Safrata, E. G. Shelley, J. McCarthy, S. M. Austin, Jr., and R. C. Barrett, Phys. Rev. **157**, 1149 (1967).
[34] R. S. Safrata, J. S. McCarthy, W. A. Little, M. R. Yearian, and R. Hofstadter, Phys. Rev. Lett. **18**, 667 (1967).
[35] F. J. Uhrhane, J. S. McCarthy, and M. R. Yearian, Phys. Rev. Lett. **26**, 578 (1971).
[36] D. G. Ravenhall and R. L. Mercer, Phys. Rev. C **13**, 2324 (1976).
[37] T. R. Fisher, J. A. Becker, B. A. Watson, H. Marshak, G. R. Burleson, M. D. Cooper, D. C. Hagerman, I. Halpern, M. J. Jakobson, R. H. Jeppeson, K. F. Johnson, L. D. Knutson, R. E. Marrs, H. O. Meyer, and R. P. Redwine, Phys. Rev. C **16**, 2367 (1977).
[38] W. C. Koehler, J. Appl. Phys. **36**, 1078 (1965).
[39] J. N. Knudson, J. D. Bowman, S. I. Penttilä, J. R. Comfort, J. Tinsley, B. G. Ritchie, J. Görgen, D. Mathis, S. S. Hanna, B. King, D. Počanić, R. A. Loveman, L. S. Fritz, and N. S. Dixon, Phys. Rev. Lett. **66**, 1036 (1991).
[40] H. W. Baer, R. D. Bolton, J. D. Bowman, M. D. Cooper, F. H. Cverna, R. H. Heffner, C. M. Hoffman, N. S. P. King, Jose Piffaretti, J. Alster, A. Doron, S. Gilad, M. A. Moinester, P. R. Bevington, and E. Winkleman, Nucl. Instrum. Methods **180**, 445 (1981).
[41] Samples produced by the Materials Preparation Center, Ames Laboratory, Iowa State University, Ames, IA, 50011.
[42] S. Gilad, Ph.D. dissertation, Tel-Aviv University, 1979.
[43] T. R. Fisher, Phys. Rev. Lett. **27**, 1078 (1971).
[44] A. Erell, J. Alster, J. Lichtenstadt, M. A. Moinester, J. D. Bowman, M. D. Cooper, F. Irom, H. S. Matis, E. Piasetzky, and U. Sennhauser, Phys. Rev. C **34**, 1822 (1986).
[45] M. A. Kelly, B. L. Berman, R. L. Bramblett, and S. C. Fultz, Phys. Rev. **179**, 1194 (1969).
[46] J. N. Knudson, J. R. Comfort, R. A. Gianelli, B. G. Ritchie, D. Rothenberger, D. Pocanic, S. S. Hanna, J. D. Bowman, H. W. Baer, A. G. Bergmann, P. A. Heusi, F. Irom, C. J. Seftor, S. Hoibraten, R. A. Loveman, S. H. Rokni, H. Crannell, D. I. Sober, W. J. Fickinger, and H. Marshak, Phys. Rev. C **35**, 1382 (1987).